



# Isometric Torque Values About Robotic Knee Using Braided Pneumatic Actuators

Ben Bolen<sup>1,\*</sup>, Lindie Burgess<sup>1</sup>, Connor Morrow<sup>1</sup>, Aidan Vogt<sup>1</sup>, Cody Scharzenberger<sup>1</sup>, Lawrence Pang<sup>1</sup>, and Alex Hunt<sup>1</sup>

<sup>1</sup> Agile and Adaptive Robotics Laboratory, Portland State University, Department of Mechanical and Materials Engineering, Portland, OR, USA

Correspondence\*:

Ben Bolen, Portland State University, Department of Mechanical and Materials Engineering, 1930 SW 4th Ave., Portland, OR, 97207, USA  
bbolen83@gmail.com

## 2 ABSTRACT

3 A lower limb model of a bipedal humanoid robot was designed to achieve biomimetic ranges  
4 of motion and isometric torque values. An important component of this robot is a biomimetic  
5 four-bar linkage knee joint that allows the joint to have two degrees of freedom (DoF) over a  
6 range of knee flexion and extension values. This joint is actuated with artificial muscles called  
7 braided pneumatic actuators (BPAs). While these artificial muscles have force-length curves that  
8 are grossly similar to real muscles, they have other limitations that need to be considered, such  
9 as their lower maximum contractile capacity and flexibility when compared to human muscles. An  
10 isometric robot knee torque stand was created to determine several things. The first task  
11 was to quantify results for actuators of different initial length and configuration. Second, use that  
12 data to characterize the difference between theoretical calculations and actual results so that we  
13 may modify the theoretical calculations. To do this, we simplified the muscle arrangement on the  
14 robotic leg so that it consists of a pair of antagonistic uniarticular flexor/extensor muscles. Another  
15 robot knee was designed using similar muscle origin insertion locations but this knee was used  
16 a simpler 1-DoF revolute joint. Testing for isometric knee torque values in these configurations  
17 allowed for the quantification of difference between measured and expected results, as well as a  
18 quantification of the factors that were important in these differences.

19 **Keywords:** BPA, Biomimetic, Function Fit, PAM, Artificial Muscle, Bioinspired, Bipedal Robot, Isometric Knee Torque

## 1 INTRODUCTION

20 Both academic researchers and the general public are keenly interested in biomimetic humanoid robots due  
21 to their many applications. In the discipline of biomimetic robotics, high fidelity humanoid robots can help  
22 improve our understanding of both human biomechanics and the underlying neuromechanical systems that  
23 control them (Shin et al., 2018; Asano et al., 2019). Experiments can be done with robots that would not be  
24 practical nor ethical if done on human test subjects, and modifying robotic platforms is a potentially faster  
25 and cheaper alternative to human observation studies.

26 For truly biomimetic humanoid robots to go a step beyond being merely bio-inspired, it is unclear how  
27 the actuator affects other aspects of the control. One requirement for proposed artificial muscle-actuators  
28 should be that they be able to produce isometric torque about humanoid joints that meets or exceeds values

29 measured in humans. There are several interesting methods of actuating robotic joints, including artificial  
30 muscles, electric motors (either directly driving the joints (**citations?**) or via cable systems (**citations?**)) ,  
31 or hydraulics. Electric motors tend to required a lot of power, generate a lot of heat, and have torque curves  
32 unlike that of real muscles. Hydraulic actuators are heavy and require a dedicated hydraulic fluid system  
33 to operate. Electrically stimulated artificial muscles are new and do not yet produce very much force.  
34 McKibben style braided pneumatic actuators (BPAs, also called Pneumatic Artificial Muscles or PAMs) are  
35 a promising method of actuation because they have low weight, high force/weight ratio, and a force-length  
36 curve that is grossly similar to actual muscle. Routing these muscles in a biomimetic arrangement can  
37 allow us to investigate and mimic the torque produced about joints by actual human muscle.

38 Previous robots that use artificial muscles do not show significant design considerations for the forces  
39 and torques that the muscles will produce. However, these aspects are critical for further understanding  
40 how muscles are controlled (**citation?**) in animals. As a consequence of this, these robots typically do  
41 not faithfully attempt to replicate the number of existing muscle actuators. They also tend to use a single  
42 degree of freedom (DoF) knee joints with a fixed position, while knees are actually better modeled as  
43 1-DoF rotating joints whose positions move as a function of knee angle (Yamaguchi and Zajac, 1989; Delp  
44 et al., 1990). They instead focus on planar, uniarticular muscle arrangements. Our research diverges from  
45 these robots by attempting to correct for these deficiencies.

46 Our previous research has laid the groundwork to start building a bipedal robot with biomimetic humanoid  
47 joints and artificial muscle actuator paths. Investigating the isometric force profile of 10 mm Festo Braided  
48 Pneumatic Actuators (BPAs, also called Pneumatic Artificial Muscle or PAMs) demonstrated artificial  
49 muscles that can be made to have a similar isometric force profile to human muscle (Hunt et al., 2017).  
50 Research on a humanoid artificial knee allowed us to build a biomimetic translating sliding knee joint  
51 (Steele et al., 2017) instead of the traditional pinned robotic joint. A more recent paper on artificial muscle  
52 attachment locations for a humanoid robot produced theoretical isometric torque curves (Bolen and Hunt,  
53 2019). Optimization of these muscle paths and attachment locations was done by Morrow to produce a  
54 torque curve and muscle path that match the robotic system more closely to the human biomechanical  
55 benchmark we are using (Morrow et al., 2020). All of the concepts can be combined to build an artificial  
56 human leg and test the validity of our theory.

57 These previous studies need to be combined and tested on a physical robot body. The 10 mm inner  
58 diameter (ID) Festo BPAs have been characterized (Hunt et al., 2017), but the 20 mm and 40 mm ID BPAs  
59 have not been. In our previous work (Bolen and Hunt, 2019; Morrow et al., 2020), moment arms have been  
60 calculated by the unit vector cross product method presented show in Hoy (Hoy et al., 1990), but not the  
61 change in muscle length over change in angle method that Hoy and others (Hoy et al., 1990; Yamaguchi  
62 and Zajac, 1989; Sherman et al., 2013; Delp et al., 1990; Seth et al., 2011) have also used. It is not known  
63 if one method is more correct than the other. Knee Instantaneous Center of Rotation (ICR) differs between  
64 the Steele model (Steele et al., 2018) and the OpenSim model Delp et al. (1990); Seth et al. (2018) model.  
65 This fact, as well as changes in the knee geometry and muscle placement, means there will be different  
66 muscle moment arms between the models. The differences in isometric torque between the theoretical,  
67 measured, and human biomechanical benchmark model need to be investigated.

68 Deviation from expected versus measured force in BPAs can happen in several ways. Festo reports  
69 that there can be a 10% deviation from theoretical force ((Corporation, 2022)). Joint friction can cause a  
70 decrease in torque, as can non-rigid elements of the artificial leg and test frame. Kinking of the artificial  
71 muscle as it wraps around a joint also is predicted to reduce the amount of available force. A further

72 reduction in force, and therefore torque, can be expected from a previously undefined reduction in force  
73 that happens as BPAs resting length is decreased.

74 We hypothesize that the isometric torque values that we measure experimentally will be lower than what  
75 is predicted by our theoretical model. A correction factor can then be applied to our calculations which will  
76 improve our results. The modified design tools we previously developed can be compared to measured  
77 isometric torque values produced by our artificial muscles about the robot knee joint, which will then be  
78 used to update how we design and analyze biomimetic joints in the future (including determining which, if  
79 any, method of calculating moment arm is the best). Future designs can then be built with artificial muscles  
80 that meet or exceed human isometric torque values.

## 2 METHODS AND MATERIALS

### 81 2.1 Overview

82 An important initial step for biomimetic humanoid robot research is to see if these robots, actuated by  
83 artificial muscles, can meet or exceed isometric torque values that are produced by human muscles. Previous  
84 research has demonstrated meeting or exceeding these human values with BPAs is at least theoretically  
85 plausible (Bolen and Hunt, 2019; Morrow et al., 2020), so the next step is to test this on an actual robot.  
86 To accomplish this, we built a jig to test if the torque produced by artificial muscles about a knee joint  
87 matches our predictions.. With the expectation that measured results will be less than theoretical, it was also  
88 necessary to simplify the robot muscle arrangement and knee design to elucidate the variables that affect the  
89 results. There are, therefore, three models that we must consider, including: (1) the human biomechanical  
90 model, (2) the conceptual robot model, and (3) the actual robot model. Within the conceptual and actual  
91 robot models, we varied the knee actuation by using either a simplified pinned knee joint or a biomimetic  
92 1-DoF knee, and muscles to either flex or extend the joint. Furthermore we varied the artificial muscle  
93 origin/insertion locations, resting lengths, diameters, and whether or not they used an artificial tendon.  
94 These results were compared to the baseline model.

95 After running these tests we also tested if the equation developed in (Hunt et al., 2017) was applicable  
96 to longer resting BPA lengths and forces in (Bolen and Hunt, 2019; Morrow et al., 2020). Comparing  
97 the discrepancy in force values expected from this equation to values we determined experimentally with  
98 additional BPA lengths, it was necessary to derive additional equations to characterize the Festo BPAs.  
99 During this process, we developed equations for maximum force in the 10 mm BPA as a function of resting  
100 length, and equations for normalized force as a function of relative strain and relative pressure in the  
101 10 mm, 20 mm and 40 mm BPAs.

### 102 2.2 Robot Architecture

103 Components of the robot leg are the knee joint, femur, tibia, BPAs, BPA end caps, artificial tendon, and  
104 attachment brackets 2. The artificial bone components are 3D printed using Onyx material on Markforged  
105 Onyx One and Mark Two printers. Onyx is a proprietary Markforged material that consists of chopped  
106 carbon fiber in nylon. Certain brackets also included carbon fiber layers to increase stiffness. Artificial  
107 tendon is made with Shimano bicycle brake cable for  $\phi$ 10 mm BPAs, and wire rope with the 20 mm and  
108 40 mm ID BPAs. When using the brake cable we first apply load to it and induce plastic deformation so  
109 that during the test the cable only has elastic deformation.

110 The goal of this investigation is to determine the isometric torque a BPA can produce in a given  
 111 configuration. Therefore the BPAs to must be inflated full pressure (which we defined as the somewhat-  
 112 standard building air supply pressure of 620 kPa). One uniarticular knee extensor and one uniarticular knee  
 113 flexor was used to actuate the joint. The joint knee tests used 10 mm internal diamter (ID) Festo BPAs. For  
 114 the biomimetic knee joint, the Biceps Femoris Short Head muscle was mimicked using a 20 mm Festo  
 115 BPA, and the vasti muscles are mimicked using one 40 mm Festo BPA. The artificial muscle is pinned  
 116 to the muscle origin location, while the other end is either pinned, or is free floating and attached to the  
 117 muscle insertion location via an artificial tendon.

118 The biomimetic robot leg assembly is for a two legged robot with 1-DoF humanoid knee joint first  
 119 introduced in (Steele et al., 2017). The 1-DoF joint with a moving Instantaneous Center of Rotation  
 120 (ICR) is achieved by using a four bar linkage mechanism. The leg assembly is based off of bones scans  
 121 of someone 6 ft tall (approx. 1.83 m) and the OpenSim Gait2392 model. Each joint is driven by two  
 122 antagonistic Festo actuators that act as artificial muscles. A test jig constrains the robot to saggital planar  
 123 motion 1. This system has two mounting locations to fix the femur to the frame. To eliminate the effect  
 124 of gravity on our test results the robot saggital plane was made parallel with the horizontal plane of the  
 125 ground.

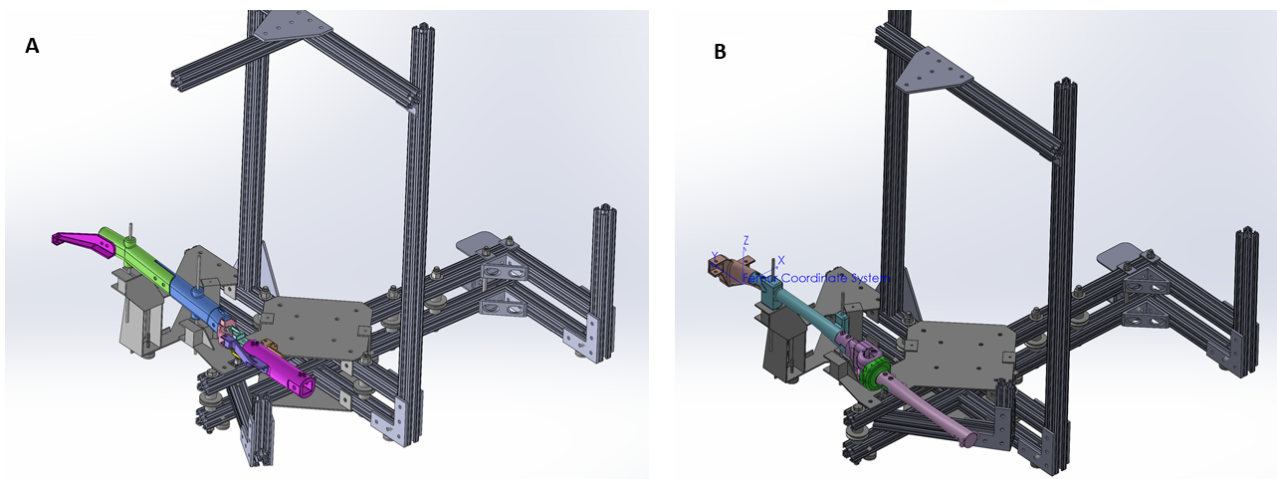


**Figure 1.** Solid model assemblies of two different robotic legs in the test stand using either (A) a revolute joint knee, or (B) a biomimetic knee.

### 126 2.2.1 Robotic Knee Joints

127 We used the sliding contact knee that was designed by Steele et al (Steele et al., 2018, 2017). The knee  
 128 is sliding contact and was designed to reduce wear. This design uses a four bar linkage that allows the  
 129 joint origin to translate in the  $\hat{x}$  and  $\hat{y}$  directions during knee rotation 3. The linkage has an Instantaneous  
 130 Center of Rotation (ICR) at the intersection of the links. To more directly compare our results with the  
 131 OpenSim model, and in the interest of simplifying our model's transformation matrices, we defined a joint  
 132 location that moved in a similar way to the human biomechanical model 3. Both models had the same  
 133 home position location, as did the pinned knee joint.

134 The differences in the knee X and Y position as a function of knee angle are shown in 4. The muscle  
 135 origin and insertion locations for each configuration is listed in 1. With the reference frames and muscle

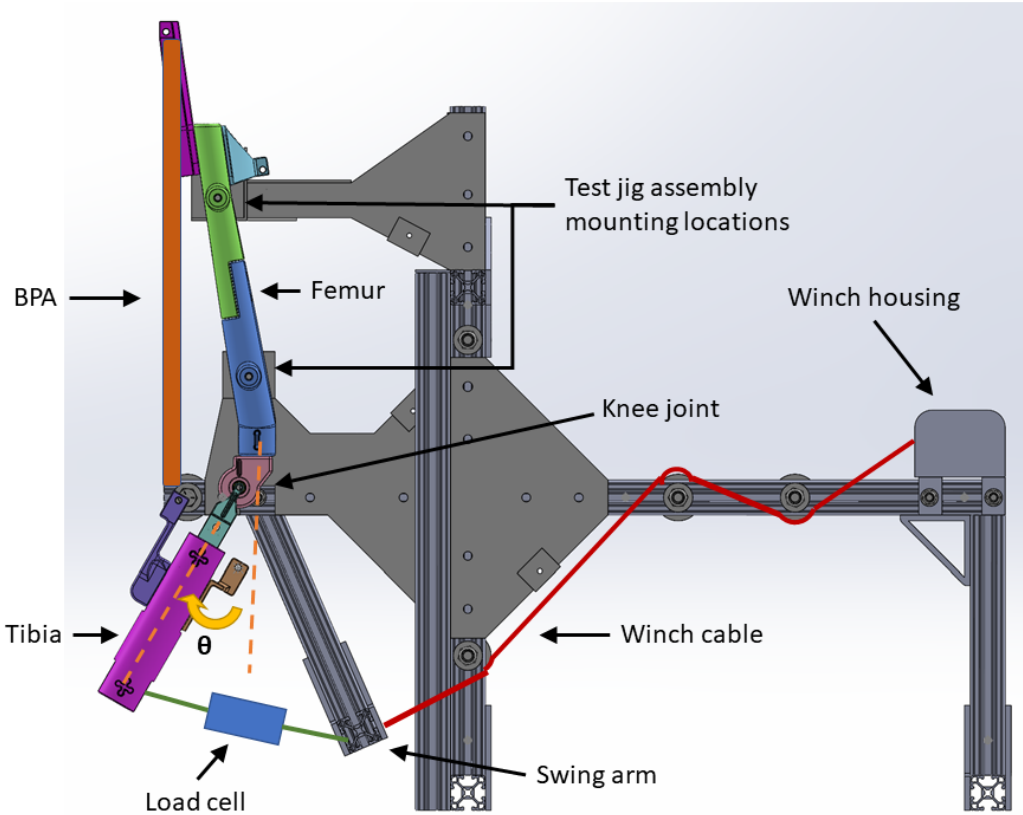


**Figure 2.** 1-DoF pinned-joint robot knee in the test apparatus with important components labeled. Leg is shown with 30 degrees flexion, i.e.  $\theta_k = -30^\circ$

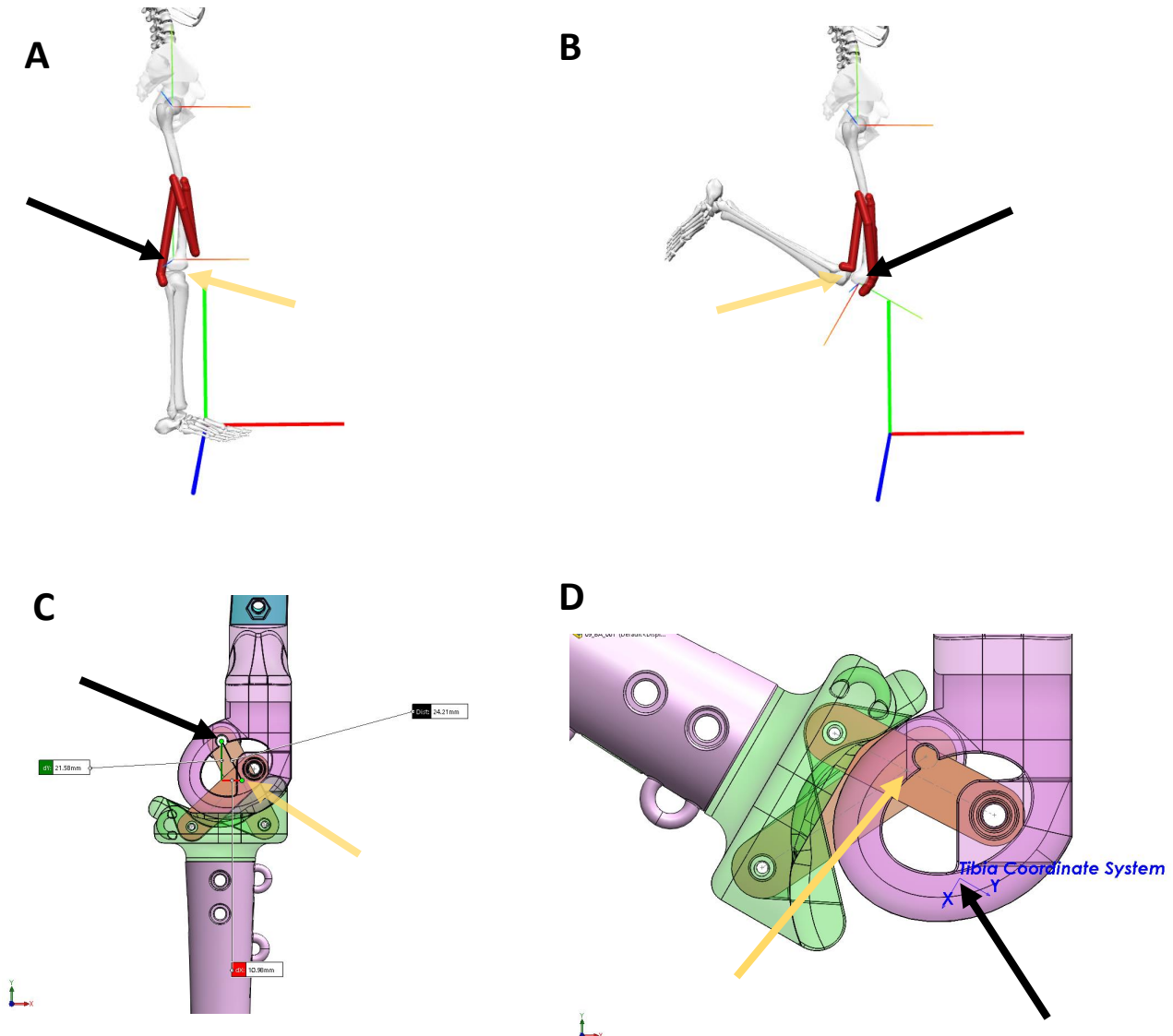
136 path geometry defined, it is then possible to calculate torque values that the muscles can produce about the  
137 joint.

### 138 2.3 Moment arm and Torque calculations

139 The goal of this study is to compare measured robot performance to both calculated robot performance  
140 and also to what we expected from a human's reported maximum isometric torque. Given a joint location  
141 and a force vector  $\vec{F}$ , there exists a distance  $\vec{d}$  from the joint to the line of action represented by  $\vec{F}$ . The  
142 classical mechanics way to calculate torque  $\vec{M}$  about the joint is to take the cross product of distance  $\vec{d}$  and  
143 force vector  $\vec{F}$  1.

$$\vec{M} = \vec{d} \times \vec{F} \quad (1)$$

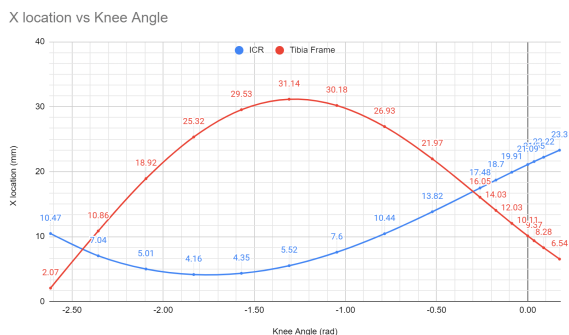
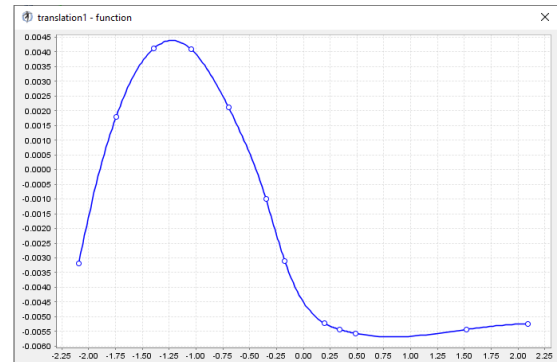
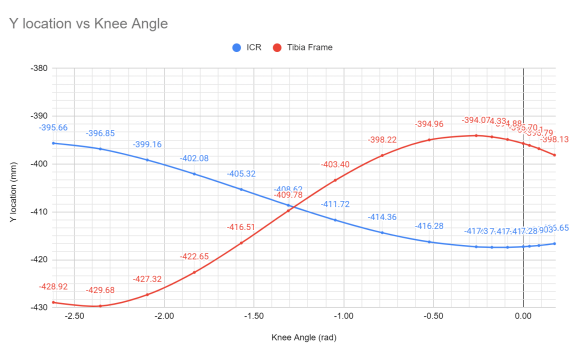
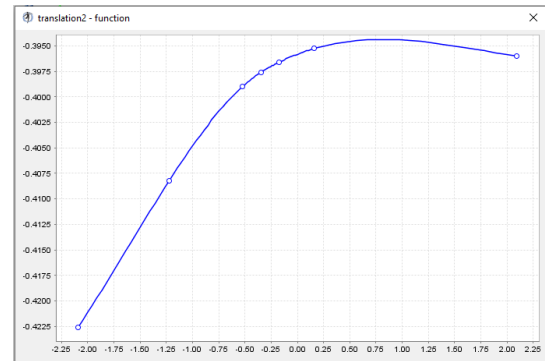
144 The calculations for human muscle force and torque that we used as a benchmark were from Delp, Hoy,  
145 Yamaguchi, Sherman, Millard, and Thelen (Delp et al., 1990; Hoy et al., 1990; Yamaguchi and Zajac, 1989;  
146 Sherman et al., 2013; Millard et al., 2013; Thelen, 2003). Reference human values were obtained using the  
147 Gait2392 model in the biomechanical modeling software OpenSim (Delp et al., 1990; Seth et al., 2011,  
148 2018). Gait2392 is the anatomical human biomechanical model used for comparison 5. Moment arm  $r_\theta$  is  
149 calculated by these sources using the following formula.



**Figure 3.** Reference frames for Gait2392 in (A) home position and (B) flexed ( $\theta = -120^\circ$ ). Frames for biomimetic robot knee in (C) home position and (D) flexed ( $\theta = -120^\circ$ ). Coordinate directions are:  $\hat{x}$  in red,  $\hat{y}$  in green, and  $\hat{z}$  in blue. Spatial frame is  $s$  and body frame is  $b$ . For (A) and (B): black arrows point to the tibia reference frame as defined by OpenSim, yellow arrows point to the actual ICR (the tibial-femoral contact point), the large axes are general space frames, and the small axes represent body frames for the hip  $h$  and knee  $k$ . For (C) and (D): black arrows point to the tibia reference frame as defined by us ( $\vec{p}_k$  is at  $\theta_3$  (see Steele et al., 2017) for details) when knee angle  $\theta_k = 0$  and follows a similar path to the Gait2392 model), yellow arrows point to the actual ICR (intersection point of the two links).

$$r_\theta = \frac{dl_m}{d\theta} \quad (2)$$

150 where  $dl$  is the change in muscle length  $l_m$  and  $d\theta$  is the change in joint angle. We opted out of using this  
 151 method. Moment arms in this study were calculated using the method developed by Young and colleagues  
 152 (Young et al., 2019). The moment arm,  $r_{\hat{k}}$ , about the  $\hat{z}$  axis is calculated by:

**A****B****C****D**

**Figure 4.** Comparison of joint X and Y positions (with respect to femur frame origin) as a function of knee angle. (A): X axis location (in millimeters) for tibial frame (red) and ICR (blue) for the biomimetic knee as a function of knee angle (in radians). (B): X axis location (in meters) for tibial frame as a function of knee angle (radians). (C): Y axis location (in millimeters) for tibial frame (red) and ICR (blue) for the biomimetic knee as a function of knee angle (in radians). (D): Y axis location (in meters) for tibial frame as a function of knee angle (radians).

$$r_{\hat{k}} = \vec{p}_{proj,i} \cdot \frac{\vec{p}_f \times \hat{k}}{\|\vec{p}_f \times \hat{k}\|} \quad (3)$$

153      $\vec{p}_{proj,i}$  is the free muscle segment projected onto the plane of interest defined by the joint axis.  $\vec{p}_f$  is the  
 154     projected muscle segment vector.

## 155 2.4 Data Collection: Equipment and Procedures

156     We built a test stand to take isometric knee torque measurements at different knee angles over its RoM.  
 157     The test stand frame is made predominantly out of 80/20 components. The knee joint is allowed to rotate  
 158     while the femur is fixed to the frame. A force sensor has one end connected to the tibia and the other is  
 159     connected to a swing arm. The swing arm is tied to the winch with 3/16 inch Kevlar rope from Quality™  
 160     Nylon Rope 3. This rope has a Kevlar core with a polyester jacket and is rated to have a break strength of  
 161     1150 lbs.



**Figure 5.** View of the human biomechanical model Gait2392 used for comparison. In this test we looked at the uniarticular muscles that attach to the femur and cross the knee, shown as red muscle actuators in the picture.

162 Force data was collected using one of two different sensors. The first was a MODERN STEP 300 kg digital  
163 crane scale. The second force sensor is a CALT DYLY-103 100 kg S shaped load cell. The was load cell was  
164 used in conjunction with a HX711 Load Cell Amplifier. Pressure data came from a Freescale MPX5700  
165 GP 5 V pressure sensor. Building air supply pressure was controlled with two pressure regulators in series.  
166 The first is a Parker model 20R113GC 0-120 *psi* pressure regulator. The second is a Husky 3/8 *in.* High  
167 Performance Air Regulator HDA72200. A Festo VTUG-10-MRCR-S1T-26V20-T516LA-UL-T532S-8K

168 valve manifold VTUG-G was used to deliver air from the pressure regulator to the actuator. This manifold  
169 is comprised of eight two-in-one bidirectional normally closed Festo VUVG-S10-T32C-AZT-M5-1T1L  
170 valves.

171 Pressure and load cell amplifier data are sent to Matlab via an Arduino Uno style Sparkfun BlackBoard  
172 C microcontroller. The computers that used Matlab were running Windows 10 and Windows 11. During  
173 phases when the Arduino was collecting force and pressure data to send to Matlab, the Arduino would also  
174 trigger (via Matlab) an onsemi 2N4401 NPN transistor to make valve manifold opened or close the valve.  
175 For other data collection the valve was manually opened and closed 7.

176 Length measurements were done using a FANUC tape measure. When there was sufficient curvature in  
177 the BPA during knee extensor torque tests, a flexible piece of string to was used to mark the axial length,  
178 and then the distance was determined with the tape measure. Other times we were able to measure the  
179 extensor length using iBayam flexible tape measures.

180 Angle measurements were taken with either a Medigauge digital electronic goniometer or with  
181 MALENOO analog goniometers of 6, 8, or 12 inch lengths. The angle of the knee joint and the angle of  
182 the force sensor to a predefined line on the tibia were the angle measurements of interest to us. The latter  
183 angle allows us to calculate torque as the force sensor was not always perpendicular with the tibial axis.

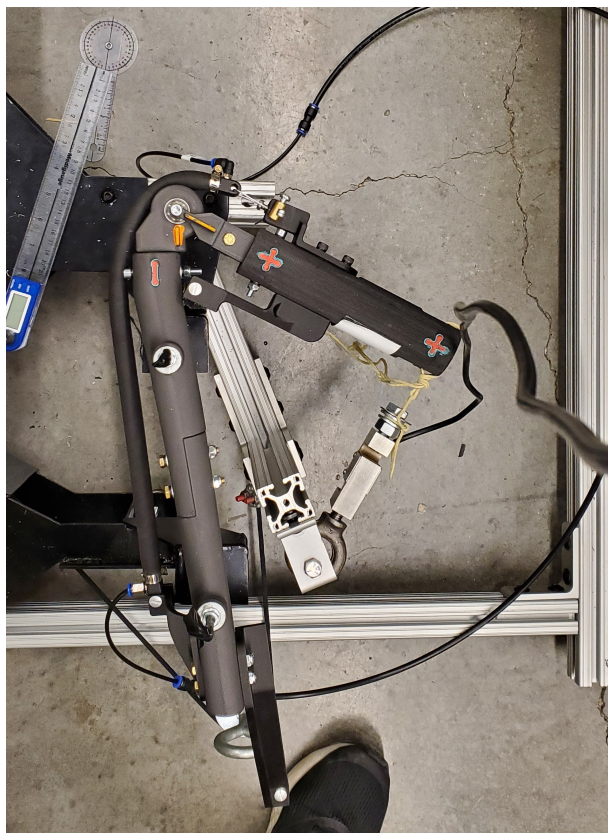


**Figure 6.** Robot leg in test jig. Setup shows the pinned knee configured for a test of the extensor BPA. The knee is positioned at  $\theta_k = -120^\circ$  flexion. The S shaped load cell attaches the tibia to the swing arm and is nearly perpendicular to the tibia in this configuration. Also note the compressed shape of the BPA during this high degree of flexion.

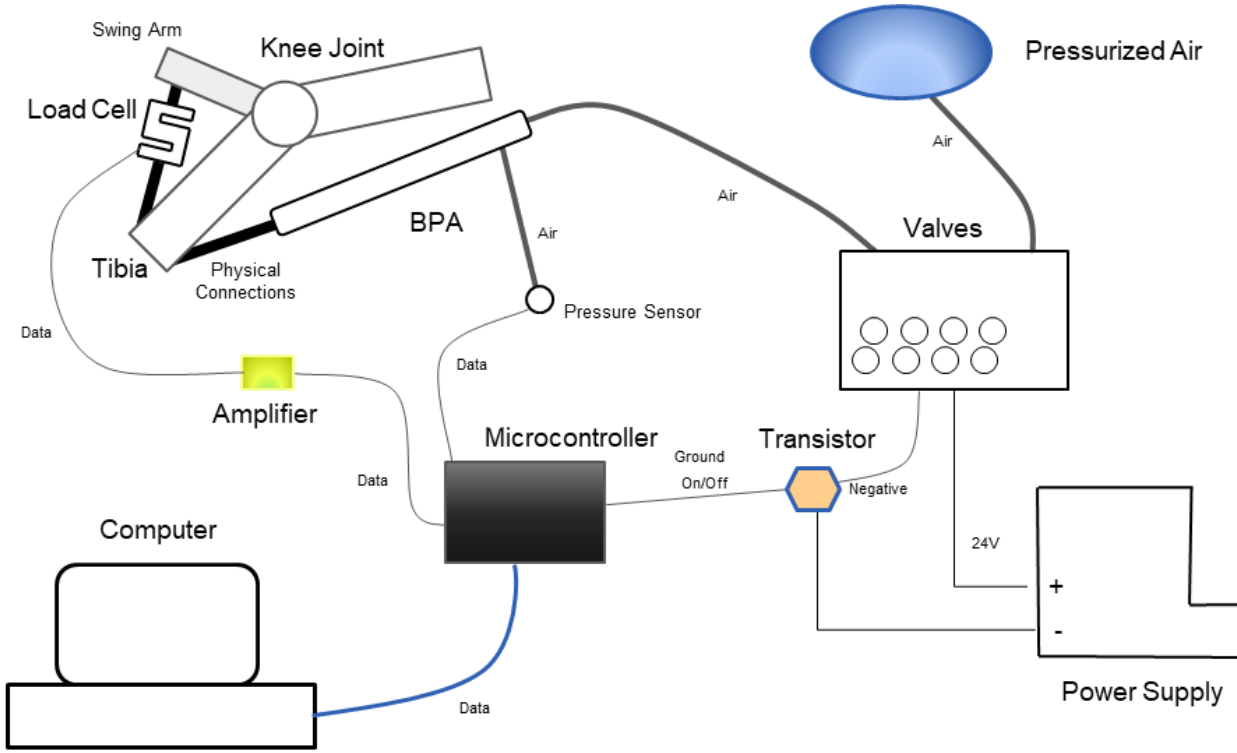


**Figure 7.** Data collection setup

## 184 2.5 Actuator Force Calculation

185 Human muscle-actuator force is calculated using the Hill muscle model. Specifically, we relied on the  
 186 equations as described by Millard (Millard et al., 2013) and used in OpenSim model Gait 2392. The  
 187 specifics equation and values are detailed in previous work by Bolen and Morrow (Bolen and Hunt, 2019;  
 188 Morrow et al., 2020).

189 BPA actuator force in our previous work has been calculated from a length-tension-pressure relationship  
 190 derived by Hunt (Hunt et al., 2017). For a given robot configuration and BPA pressure  $P$  (in kPa), the  
 191 scalar force  $F$  (in Newtons) for each of the artificial muscles can be determined by solving the equation:

$$P = 254 \text{ kPa} + 1.23 \frac{\text{kPa}}{N} \cdot F + 15.6 \text{ kPa} \cdot S + 192 \text{ kPa} \cdot \tan \left( 2.03 \left( \frac{\epsilon}{-0.331 \times 10^{-3} \frac{1}{N} \cdot F + \epsilon_{max}} - 0.46 \right) \right) \quad (4)$$

192  $\epsilon$  is the amount of contraction, and  $\epsilon_{max}$  is the maximum amount of contraction in a BPA without external  
 193 load that is inflated to 620 kPa.  $S$  is the hysteresis factor of the artificial muscle in which  $S = 1$  indicates  
 194 the muscle is shortening and with  $S = -1$  it is lengthening. For isometric contraction, set  $S = 0$ . An  
 195 important note for (4) is that the coefficients have been updated with the correct values. We used this  
 196 corrected version of the equation to create a lookup table for actuator force for a given amount of pressure  
 197 and relative strain  $\epsilon^*$ , defined as

$$\epsilon^* = \frac{\epsilon}{\epsilon_{max}} \quad (5)$$

With this lookup table created it is possible to use a curve fit to develop an equation for force as a function of pressure and relative strain. However, we note here two problems with the BPA characterization in (Hunt et al., 2017). The first is that this testing was done with a maximum of 111.2 N applied load, which is only about 20% of the maximum isometric force the Festo BPA is rated for at maximum pressure and no contraction. Secondly, we observed that maximum force in the BPAs decrease as the resting length decreases. Therefore, we created a test jig apparatus to test isometric force for various resting lengths of 10 mm Festo BPAs at different pressures.

Each BPA resting length,  $l_{rest}$ , is measured as the distance between the hose clamps. This is how Festo defines  $l_{rest}$ , although in (Hunt et al., 2017) it was measured to also include end cap length. We then inflated each BPA to maximum pressure ( $P_{max} = 620$  kPa) and measured  $\epsilon_{max}$ . The BPAs were then deflated, placed vertically in the test jig made out of 80/20 pieces and fixed between two crossmembers. The force sensor was placed between the upper crossmember and the BPA. For 120 mm, 220 mm, 260 mm, 281 mm and 281 mm resting lengths, a Loadstar RAS1-01KS-S\*C00 S Shaped load cell was used instead of the other force sensors previously mentioned. The distance between the crossmembers was adjusted to get different amounts of  $\epsilon^*$ . The BPAs would then be inflated. BPAs with 120 mm, 220 mm, 260 mm, 281 mm and 281 mm resting lengths had a lot of  $P$  variation, with only 4-5 different values of  $\epsilon^*$  per BPA. Conversely, BPAs with resting lengths of 112 mm, 415 mm, 455 mm, 490 mm and 518 mm had many different values of  $\epsilon^*$  recorded, but all values were taken at or near  $P_{max}$ . Force and pressure data was collected as described in a previous section, above.

### 3 RESULTS

217 Results from BPA characterization tests are shown first in 8. Fig. 8A and 8B show a force response  
 218 resembling an arctan curve along the resting length dimension and with a more linear response along the  
 219 pressure axis. We used a surface fit to find the equation for maximum force in a  $\phi 10$  mm BPA as a function  
 220 of resting length and pressure, i.e.  $F_{max_{10}}(l_{rest}, P)$ .

$$F_{max_{10}}(l_{rest}, P) = a1 \cdot P \cdot \arctan(a2 \cdot P \cdot (l_{rest} - 0.0075)) \quad (6)$$

221  $l_{rest}$  is offset by 7.5 mm because solid modeling showed our end caps contact each other at this  
 222 resting length. Therefore  $F_{max_{10}}(7.5 \text{ mm}) = 0$  because air would flow in one endcap and out the other  
 223 (assuming perfect alignment). The curve fitting was done using the Nonlinear Least Squares method  
 224 and a Least Absolute Residual robustness.  $a1 = 0.4848 \text{ N kPa}^{-1}$  (0.4848–0.488 with 95% CI) and  
 225  $a2 = 0.03306 \text{ kPa}^{-1} \text{ m}^{-1}$  (0.0325–0.03362 with 95% CI). 6 has an Adjusted  $R^2 = 0.9997$  and an  
 226 RMSE = 2.749. Substituting  $P_{max} = 620 \text{ kPa}$  into 6 yields the following simplified equation:

$$F_{max_{10}}(l_{rest}) = 301.6 \text{ N} \cdot \arctan(20.5 \text{ m}^{-1} \cdot (l_{rest} - 0.0075)) \quad (7)$$

227 Equation 7 is compared with the data in 8B. It can be seen that  $\lim_{l_{rest} \rightarrow \infty} F_{max_{10}} = 473.7 \text{ N}$ . Fig. 8C shows  
 228 an attempt at a linear fit for  $\epsilon_{max}(l_{rest})$ . There was a large amount of variance in the data, with the linear  
 229 fit giving an adjusted  $R^2 = 0.4124$  and an RMSE = 0.0083, therefore at this time we cannot say with  
 230 confidence that there is a relationship between maximum strain and resting length.

231 The next step in BPA characterization we derived an equation for normalized force in the BPA, or  
 232  $F^* = F/F_{max}$ . In previous work we have already used relative strain  $\epsilon^* = \epsilon/\epsilon_{max}$ , and here we will  
 233 also introduce relative pressure  $P^* = P/P_{max}$ . Then we can show that  $F^*(\epsilon^*, P^*)$  9. By visualizing the  
 234 lookup tables discussed above, and the Festo Corporation data sheet, we can see that there appears to be  
 235 an exponential relationship between  $\epsilon^*$  and  $F$ , and a linear relationship between  $P$  and  $F$ . A polynomial  
 236 surface fit also shows an interaction between the linear  $P$  and exponential  $\epsilon^*$  terms. Therefore we fit a  
 237 surface to the original data using an equation of the form

$$F^*(\epsilon^*, P) = b0 + \exp(-b1 \cdot \epsilon^*) + b2 + P \exp(-b3 \cdot (\epsilon^*)^2) + b4 + b5 \cdot P^* \quad (8)$$

238 With all the additional data collected on 10 mm ID BPAs with resting lengths given in 8, we then  
 239 normalized the force data collected by dividing each BPA's force results by  $F_{max_{10}}$  for that BPA. Pressure  
 240 data was divided by  $P_{max}$ . This reduced much of the variance in the data, as shown in Fig. 9, which  
 241 qualitatively pointed towards using a surface fit as the right approach for  $F^*$ . Using  $\epsilon^*$  and  $P^*$ , it was  
 242 possible to reduce the amount of coefficients in Eq. 8 from six to only two. The equation for normalized  
 243 force is

$$F^*(\epsilon^*, P^*) = -1 + \exp(-c1 \cdot \epsilon^*) + P^* \cdot \exp(-c2 \cdot (\epsilon^*)^2) \quad (9)$$

244 with  $c1 = 1.7$  (1.692–1.708 with 95% CI) and  $c2 = 0.2$  (0.1968–0.2029 with 95% CI). This surface fit  
 245 was done using Nonlinear Least Squares method and Least Absolute Residuals robustness. Additional data  
 246 from separate tests using the 120 mm, 220 mm, 260 mm, 281 mm and 281 mm resting lengths were used

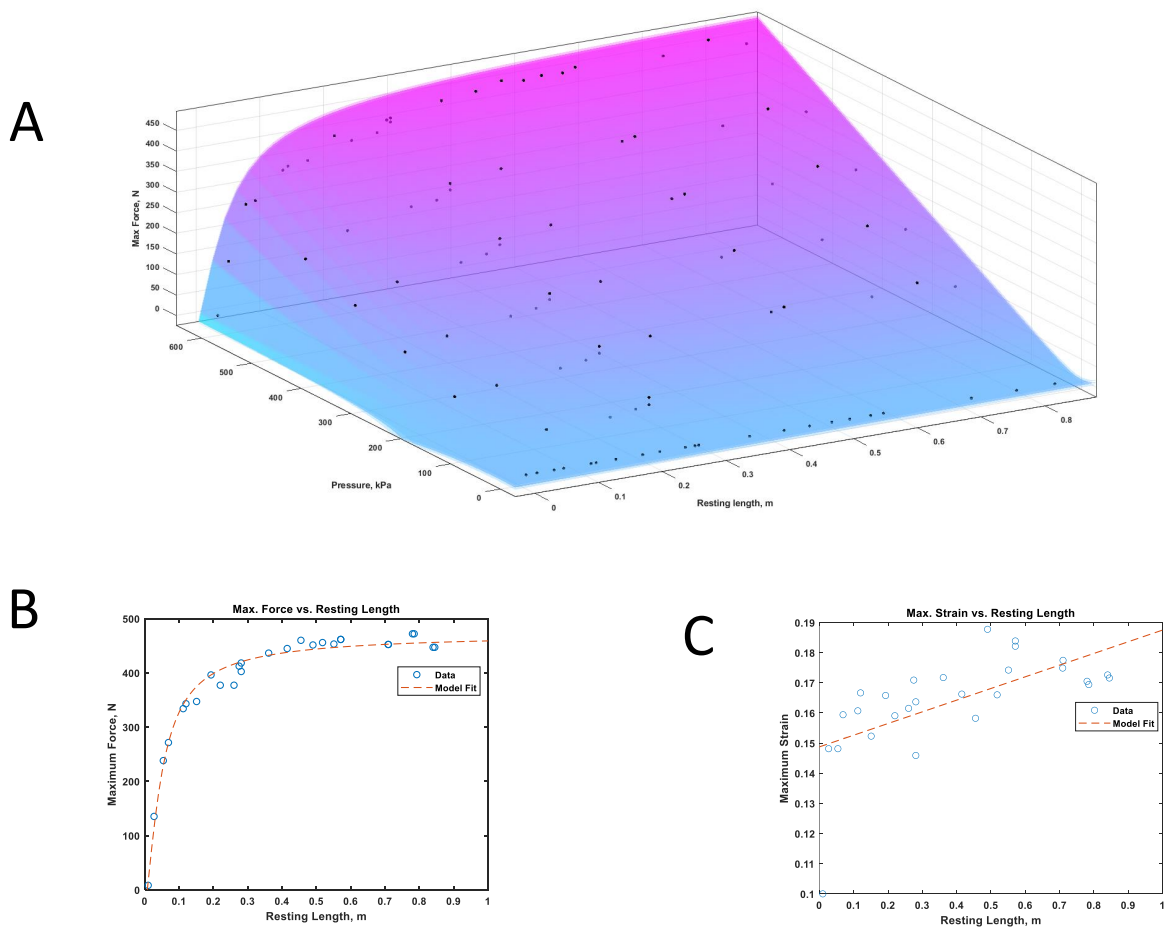


**Figure 8.** Results for finding the relationship between  $l_{rest}$  and  $F_{max10}$ ,  $\epsilon_{max}$ . **(A)** Surface fit for  $F_{max10}(l_{rest}, P)$ . **(B)**  $F_{max10}$  versus  $l_{rest}$  at  $P_{max} = 620$  kPa. **(C)**  $\epsilon_{max}$  versus  $l_{rest}$  at  $P_{max} = 620$  kPa. No conclusive relationship between  $\epsilon_{max}$  and  $l_{rest}$  could be deduced from this experiment.

247 for validation. Eq. 9 has an Adjusted  $R^2 = 0.9998$ , SSE = 0.007833, and an RMSE = 0.0057. Validation  
 248 SSE = 0.482595 and RMSE = 0.044292. Combining Eq. 9 and Eq. 7 will now allow researchers to  
 249 determine the force  $F$  in a BPA given  $l_{rest}$ ,  $P$ , and  $\epsilon^*$ .

$$F(\epsilon^*, P^*, l_{rest}) = F^*(\epsilon^*, P^*) \cdot F_{max}(l_{rest}) \quad (10)$$

250 Force functions for  $\phi 20$  mm and  $\phi 40$  mm BPAs were also derived. Isometric force tests were not  
 251 performed on these BPA sizes. Instead, values of  $F_{max20} = 1500$  N,  $F_{max40} = 6000$  N,  $\epsilon_{max} = 25\%$ ,  
 252 and  $P_{max} = 600$  kPa, provided by Festo Corporation (Corporation, 2022) were used. The normalized for  
 253 equation for the  $\phi 20$  mm BPA is

$$F^*(\epsilon^*, P^*) = -0.1881 + \exp(-7.965 \cdot \epsilon^* - 1.677) + P \cdot \exp(-2.036 \cdot (\epsilon^*)^2) - 0.1518 + 0.1518 \cdot P^* \quad (11)$$

254 From this equation, it can be seen that the coefficient  $b4 = -b5$ . Eq. 11 has an Adjusted  $R^2 = 0.9985$ ,  
 255 SSE = 0.0125, and an RMSE = 0.0154. The  $\phi 40$  mm BPA fit equation is

$$F^*(\epsilon^*, P^*) = -0.06974 + \exp(-8.547 \cdot \epsilon^* - 2.6287) + P \cdot \exp(-0.2854 \cdot (\epsilon^*) + 1.148 - 2.128 \cdot P^*) \quad (12)$$

256 It can be seen that 12 is similar to the structure of Eqns. 8 and 11, but with an  $\epsilon^*$  term in the second  
 257 exponential instead of  $\epsilon^{*2}$ . Eq. 12 has an Adjusted  $R^2 = 0.9999$ , SSE =  $8.614 \times 10^{-4}$ , and an RMSE =  
 258 0.0040.

259 The new method of calculating 10 mm BPA force is used to calculate maximum isometric torque for the  
 260 various configurations. Starting with the simplest case, we examine BPAs of 45.7 cm and 48.5 cm resting  
 261 lengths on the pinned knee used for knee flexion 10. Fig. 10A shows measured torque as blue diamonds and  
 262 expected (theoretical) torque as a magenta line. Experimentally measured values of BPA length, pressure,  
 263 and moment arm were used with Eq. 10 to back calculate torque values. It was determined that a major part  
 264 of the discrepancy in measured versus expected torque values was due to differences in measured versus  
 265 expected  $\epsilon^*$  values (Fig. 10B). After running an optimization algorithm to change the length of the end cap  
 266 fitting, Fig. 10C shows improved results. The results of the optimization were validated with the 45.7 cm  
 267 isometric torque values 10D. The fitting length in the algorithm is changed from 25.4 mm to 35.2 mm. The  
 268 optimization yielded an SSE = 554.6 and the validation returned a SSE = 315.3 with a RMSE = 2.96.

269 Pinned knee extensor results using 10 mm ID Festo BPAs of 41.5 cm, 45.7 cm and 48.5 cm resting lengths  
 270 are shown in Fig. 11. Measured torque was slightly higher than expected in the 48 cm BPA whereas it was  
 271 slightly lower than expected in the 45.7 cm BPA. The 41.5 cm BPA was used in two configurations: with  
 272 and without an artificial tendon. Previous optimization wasn't used with these results.

273 Why the discrepancy between the results? The first two seem acceptable, but not perfect. The shorter  
 274 the resting length, the more the results are less than expected. Comparing measured values of  $l_m$  and  
 275  $\epsilon^*$  to theoretical shows a close correlation, but would increase torque for the first two and decrease for  
 276 the second. The BPA w/ artifical tendon shows a discrepancy, so maybe the tendon length was measured  
 277 incorrectly? Well, maybe looking at Fig. again can shed some insight? It would be possible to bring it  
 278 into the Matlab image acquisition toolbox to analyze lengths. If I can also show somehow that the shorter  
 279 lengths tend to kink then that would also let us create a nonlinear torque correction factor along the lines of  
 280  $M_{\hat{k}} = r\bar{k} \times (F - cf \cdot F \cdot \theta_k)$ . Improved solid model might also help?

281 Fig. 12 shows the results optimized flexor calculation method in the biomimetic knee for a 10 mm ID  
 282  $l_{rest} = 41.5cm$  BPA with a 12 mm artificial tendon made out of Shimano bicycle brake cable. Comparing  
 283 the previous method of calculating torque to the measured torque results in an SSE = 287.3 and an  
 284 RMSE = 5.36. The optimized torque calculation fits much better with a SSE = 1.282 and a RMSE =  
 285 0.358. Experimentally measured values were again used to back calculate torque, although we note that  
 286 moment arm  $r_{\hat{k}}$  was measured from knee ICR, not  $p_k$ , and that experimentally measuring  $r_{\hat{k}}$  is less precise  
 287 ( $\pm 5$  mm) in the biomimetic knee versus the pinned knee.

288 We obtained results for isometric torque in ?? using the biomimetic knee with a  $\phi 10$  mm BPA in the  
 289 extensor configuration. The torque values differ a lot from those we expected. Looking at 13B it can be  
 290 obsereveed that the length is very close to what we expected, but 13C. However, again we note that moment  
 291 arm by hand is measured to the ICR, and using this value would mean we would expect even high torque

292 than what was observed. Fig.14 shows the difficulty of modeling something that passes through the femoral  
293 condyles.

294 Opensim comparison. Full size BPAs in biomimetic knee assembly results.

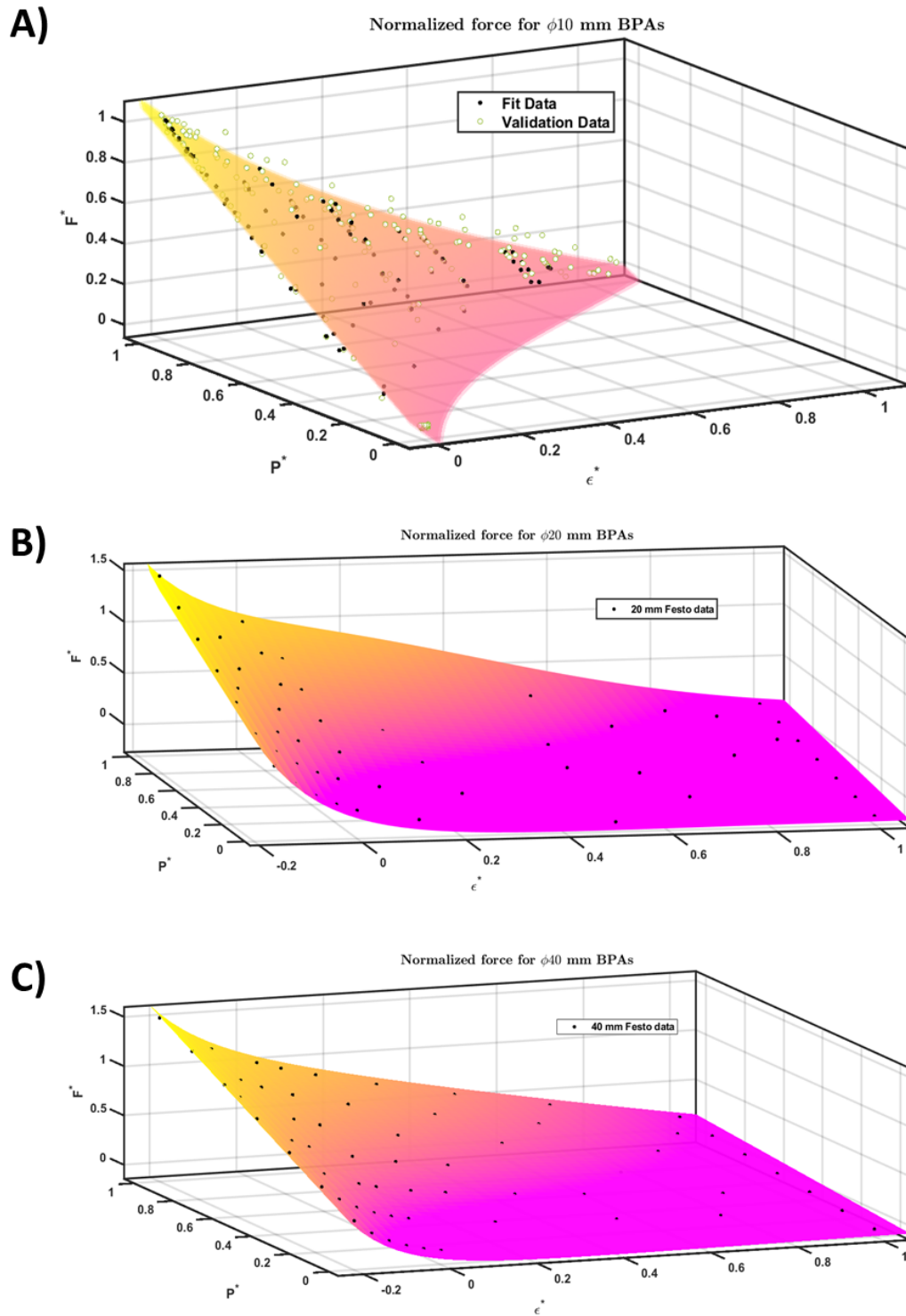


**Figure 9.** Surface fit for  $F^*(\epsilon^*, P^*)$  with (95% CI shown). Black circles represent fit data. **(A)** Fit data for  $\phi 10$  mm Festo BPA. Validation data is the green circles. **(B)** Fit data for  $\phi 20$  mm Festo BPAs. **(C)** Fit data for  $\phi 40$  mm Festo BPAs.

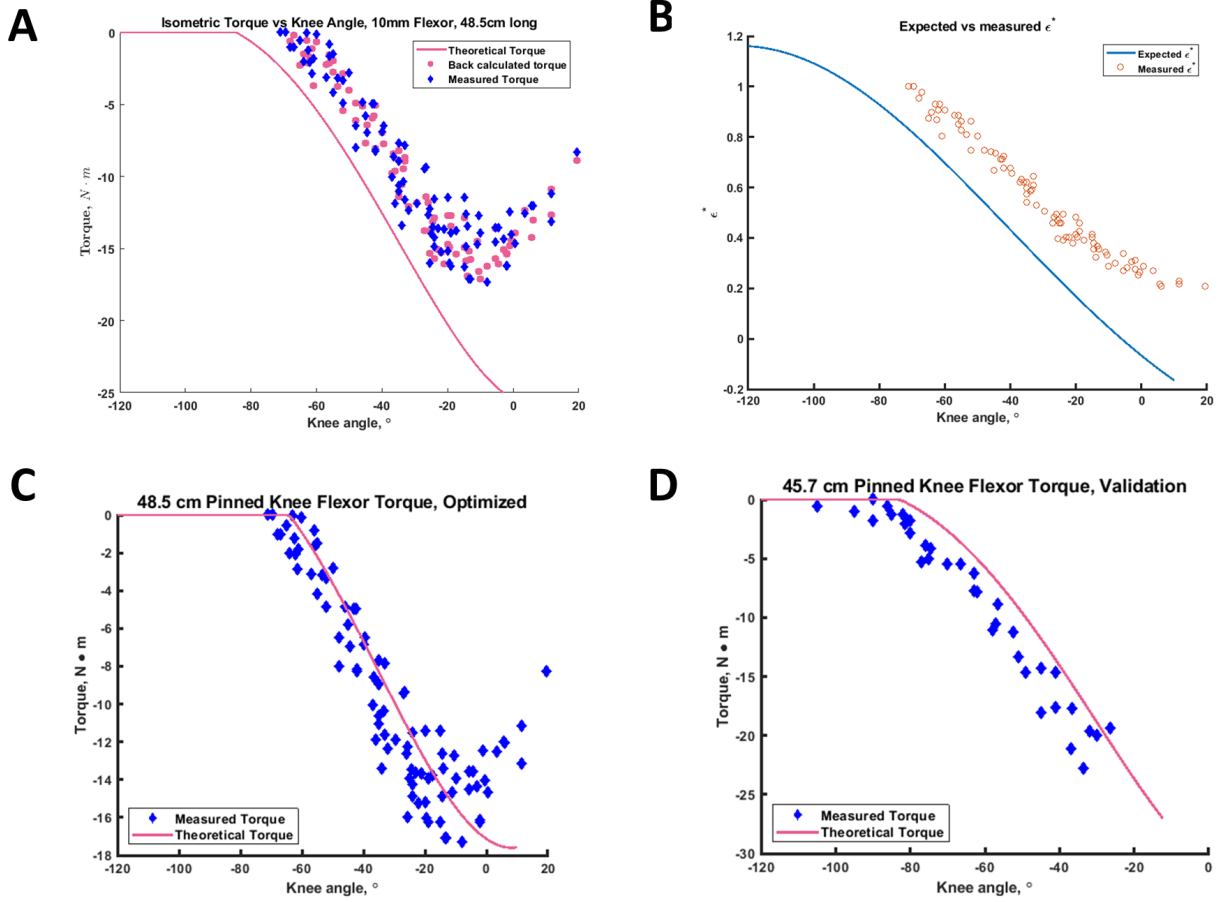


**Figure 10.** Results for the pinned knee using flexor BPAs. **(A)** Theoretical, measured, and back calculated torque for the 48.5 cm BPA. **(B)** comparison of measured versus expected  $\epsilon^*$  for the 48.5 cm BPA. **(C)** Theoretical and measured torque for the 48.5 cm BPA using an optimized fitting length of 35.2 mm. **(D)** Theoretical and measured torque for the 45.7 cm BPA using an optimized fitting length of 35.2 mm

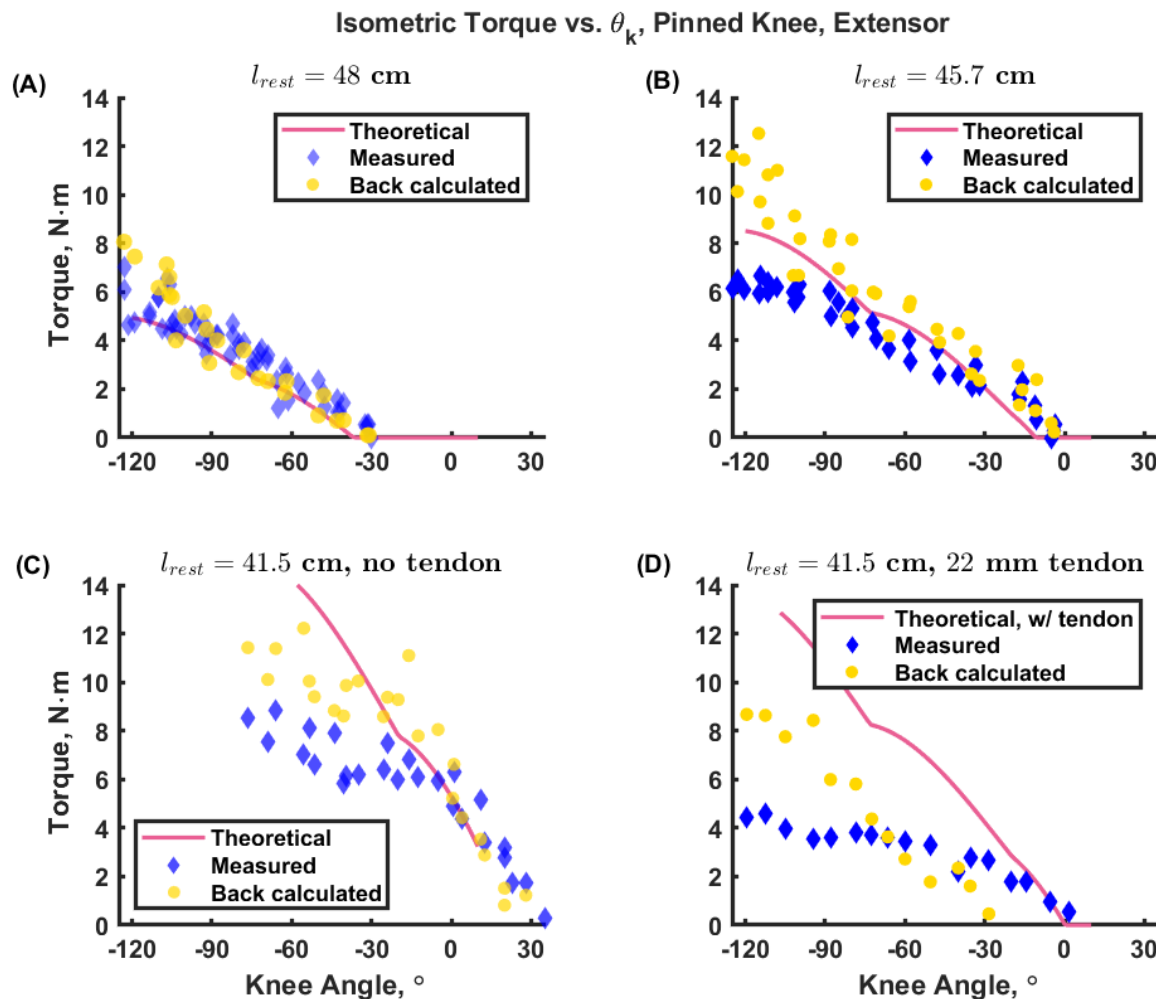


**Figure 11.** Pinned knee isometric torque with the extensor BPA for lengths, **(a)** 48.5 cm, **(A)** 45.5 cm, **(c)** 41.5 cm, and **(D)** 41.5 cm with a 22 mm tendon

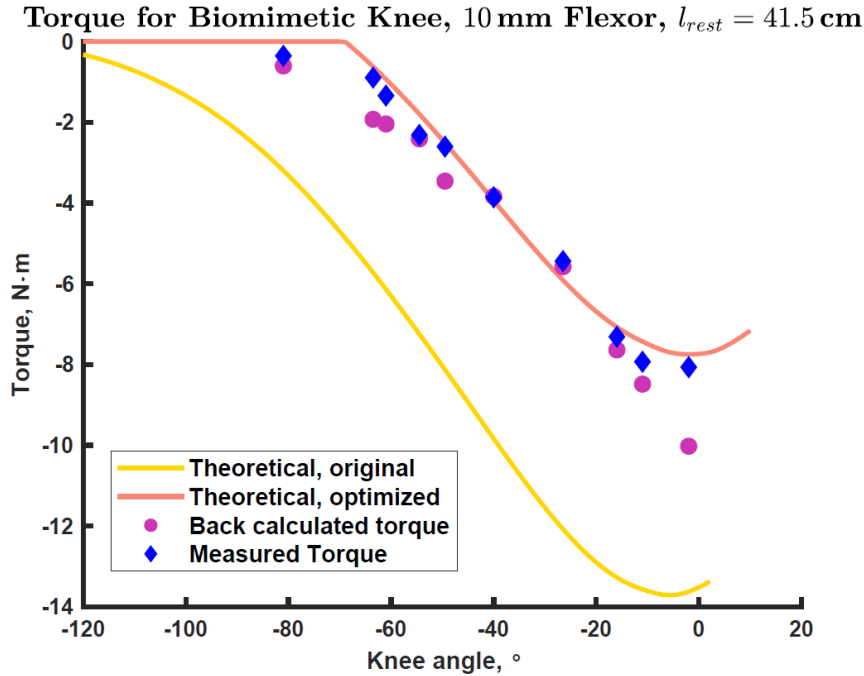


**Figure 12.** Biomimetic knee isometric torque for a 10 mm ID  $l_{rest} = 41.5 \text{ cm}$  flexor BPA with a 12 mm artificial tendon. Blue diamond shows the measured torque values. Light orange line shows the theoretical torque expected using the updated actuator force equation and the optimized fitting length. The yellow line shows the theoretical torque expected using without the optimized fitting length. Magenta circles are torque values back calculated from experimentally measured values of  $l_m$ ,  $P$ , and  $r_k$  (using measurements from knee ICR not  $p_k$ ).

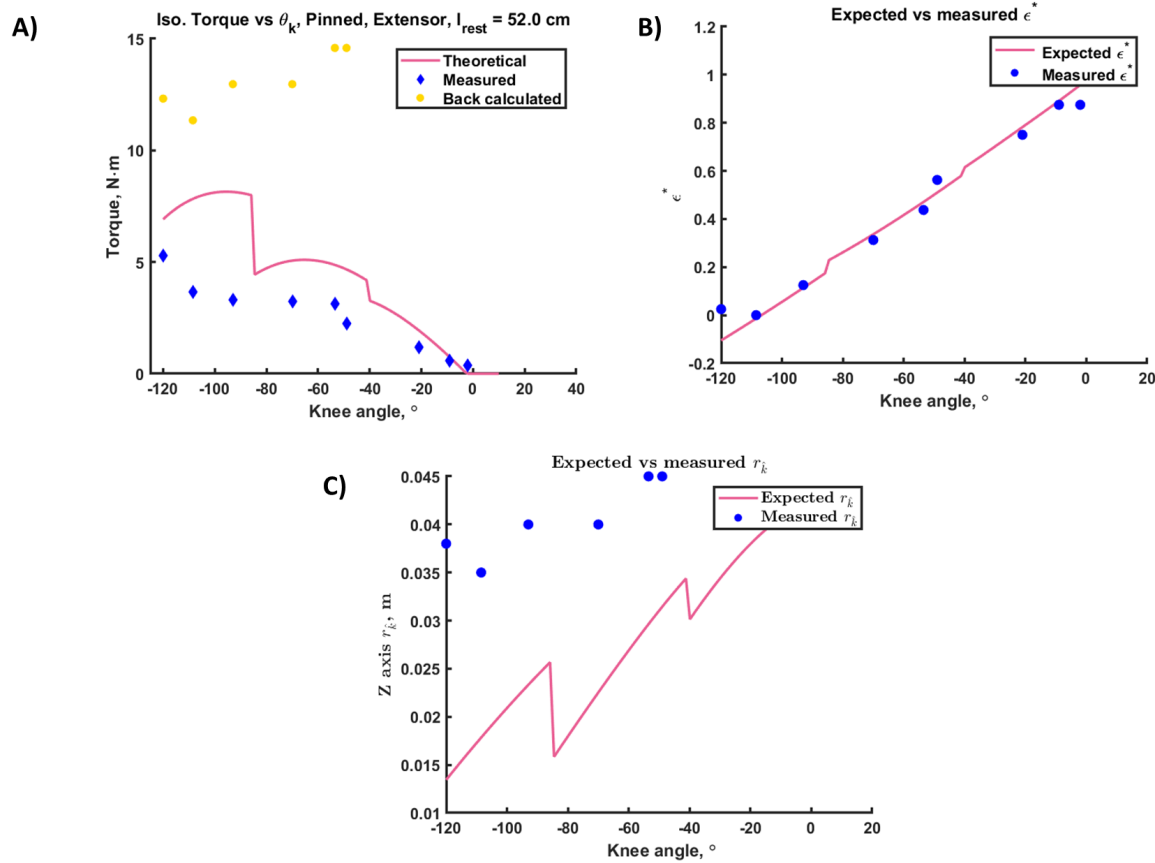


**Figure 13.** Measured versus expected results using a  $\phi 10$  mm,  $l_{rest} = 51.8$  cm extensor BPA on the biomimetic knee. **A** Isometric Torque. **B** Relative Strain. **C** moment arm.



**Figure 14.** A configuration that is particularly hard to model.

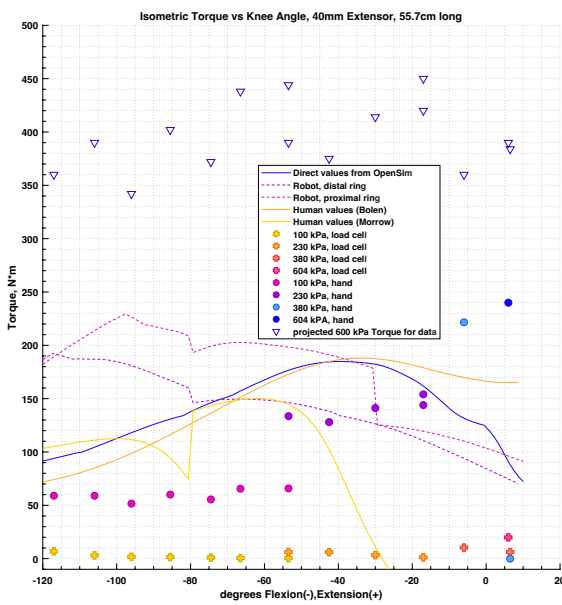


**Figure 15.** Comparison of isometric torque for theoretical BPA values with the humanoid knee, human muscle calculations using our method, and human muscle values as provided by OpenSim. Configurations listed are for (A) flexor and (B) extensor muscles. Note the major discrepancies between the our human value and OpenSim's, which calls into question the accuracy of our calculations.

## 4 DISCUSSION

295 The analysis in this study has allowed us to create novel equations for calculating force in BPAs of  
296 10 mm(Eqs. 7,9) ID.

297 There certainly are many factors that affect the isometric torque results. Compliance in testing system,  
298 flexibility of brackets, imperfect modeling, variation in individual BPAs.

299 Simplifying the model and testing it allowed us to see how we were deficient in our previous analysis.  
300 The isometric system is not rigid. It adds springiness, not

301 Curving BPA during high angles of knee flexion show the BPA being stretched and compressed. It is  
302 known that the axial stress in a pressure vessel is

$$\sigma_z = \frac{F}{A} = \frac{Pd^2}{(d + 2t)^2 - d^2} \quad (13)$$

303 Where  $\sigma_z$  is the axial stress,  $F$  is Force,  $A$  is area,  $P$  is the internal pressure,  $t$  is the wall thickness, and  $d$   
304 is the mean diameter ( $O.D. - t$ ). In thin wall pressure vessels 13 can be reduced to

$$\sigma_z = \frac{Pd}{4t} \quad (14)$$

## RESOURCE IDENTIFICATION INITIATIVE

## CONFLICT OF INTEREST STATEMENT

305 The authors declare that the research was conducted in the absence of any commercial or financial  
306 relationships that could be construed as a potential conflict of interest.

## AUTHOR CONTRIBUTIONS

307 BB, CM, and AH contributed to conception and design of the study. BB and CM wrote the code to calculate  
308 theoretical human and robot isometric torques. Figures were created by BB and AV. BB, LB, and AV wrote  
309 code for data collection and analysis. BB collected the data and performed the statistical analysis. BB  
310 organized the database. BB wrote the first draft of the manuscript. BB, LB, and AH wrote sections of the  
311 manuscript. All authors contributed to manuscript revision, read, and approved the submitted version.

## FUNDING

312 Research for this article was funded by the Department of Mechanical and Materials Engineering at  
313 Portland State University, the National Science Foundation (NSF) grant for NeuroNex: Communication,  
314 Coordination, and Control in Systems (C3NS) 2015317 and NSF grant 1943483.

## ACKNOWLEDGMENTS

315 The authors would like to acknowledge the contribution of Alex Steele, who designed the initial biomimetic  
316 4-bar knee linkage we used for the test. He gave us solid models, built a 3D prototype, and let us break said  
317 prototype. His prompt and thoughtful responses to our questions about the previous design was very much  
318 appreciated. The authors would also like to thank Jasmine Bradley for her help reworking the figures in the  
319 results section. As a visual designer, her contributions improved the aesthetic quality of the images. She  
320 also helped us choose colors that ensured data accessibility for people with color blindness.

## SUPPLEMENTAL DATA

321 Supplemental Data includes figures for the test setup.

## DATA AVAILABILITY STATEMENT

322 The data sets are available from the authors upon request.

## REFERENCES

- 323 Asano, Y., Okada, K., and Inaba, M. (2019). enMusculoskeletal design, control, and application of human  
324 mimetic humanoid Kenshiro. *Bioinspiration & Biomimetics* 14, 036011. doi:10.1088/1748-3190/ab03fc  
325 Bolen, B. P. and Hunt, A. J. (2019). enDetermination of Artificial Muscle Placement for Biomimetic  
326 Humanoid Robot Legs. In *Biomimetic and Biohybrid Systems*, eds. U. Martinez-Hernandez, V. Vouloussi,  
327 A. Mura, M. Mangan, M. Asada, T. J. Prescott, and P. F. Verschure (Cham: Springer International  
328 Publishing), vol. 11556. 15–26. doi:10.1007/978-3-030-24741-6\_2  
329 [Dataset] Corporation, F. (2022). Festo Fluidic Muscle DMSP

- 330 Delp, S., Loan, J., Hoy, M., Zajac, F., Topp, E., and Rosen, J. (1990). enAn interactive graphics-based  
331 model of the lower extremity to study orthopaedic surgical procedures. *IEEE Transactions on Biomedical  
332 Engineering* 37, 757–767. doi:10.1109/10.102791
- 333 Hoy, M., Zajac, F., and Gordon, M. (1990). A musculoskeletal model of the human lower extremity: the  
334 effect of muscle, tendon, and moment arm on the moment-angle relationship of musculotendon actuators  
335 at the hip, knee, and ankle. *Journal of Biomechanics* 23, 157–169
- 336 Hunt, A., Gruber-Tilton, A., and Quinn, R. (2017). Modeling length effects of braided pneumatic actuators.  
337 In *IDETC/CIE 2017* (Cleveland, OH: ASME)
- 338 Millard, M., Uchida, T., Seth, A., and Delp, S. L. (2013). enFlexing Computational Muscle: Modeling  
339 and Simulation of Musculotendon Dynamics. *Journal of Biomechanical Engineering* 135, 021005.  
340 doi:10.1115/1.4023390
- 341 Morrow, C., Bolen, B., and Hunt, A. (2020). enOptimization of Artificial Muscle Placements for a  
342 Humanoid Bipedal Robot. In *Biomimetic and Biohybrid Systems*
- 343 Seth, A., Hicks, J. L., Uchida, T. K., Habib, A., Dembia, C. L., Dunne, J. J., et al. (2018). enOpenSim:  
344 Simulating musculoskeletal dynamics and neuromuscular control to study human and animal movement.  
345 *PLOS Computational Biology* 14, e1006223. doi:10.1371/journal.pcbi.1006223
- 346 [Dataset] Seth, A., Sherman, M., Reinbolt, J. A., and Delp, S. L. (2011). OpenSim: a musculoskeletal  
347 modeling and simulation framework for in silico investigations and exchange.
- 348 Sherman, M. A., Seth, A., and Delp, S. L. (2013). enWhat is a Moment Arm? Calculating Muscle  
349 Effectiveness in Biomechanical Models Using Generalized Coordinates. In *Volume 7B: 9th International  
350 Conference on Multibody Systems, Nonlinear Dynamics, and Control* (Portland, Oregon, USA: American  
351 Society of Mechanical Engineers), V07BT10A052. doi:10.1115/DETC2013-13633
- 352 Shin, H., Ikemoto, S., and Hosoda, K. (2018). Constructive understanding and reproduction of functions  
353 of gluteus medius by using a musculoskeletal walking robot. *Advanced Robotics* 32, 202–214. doi:10.  
354 1080/01691864.2018.1434015. Publisher: Taylor & Francis
- 355 Steele, A., Hunt, A., and Etoundi, A. (2018). Biomimetic Knee Design to Improve Joint Torque and Life  
356 for Bipedal Robotics (Bristol, UK)
- 357 Steele, A. G., Hunt, A., and Etoundi, A. C. (2017). enDevelopment of a Bio-inspired Knee Joint Mechanism  
358 for a Bipedal Robot. In *Biomimetic and Biohybrid Systems* (Springer, Cham), Lecture Notes in Computer  
359 Science, 418–427. doi:10.1007/978-3-319-63537-8\_35
- 360 Thelen, D. G. (2003). enAdjustment of Muscle Mechanics Model Parameters to Simulate Dynamic  
361 Contractions in Older Adults. *Journal of Biomechanical Engineering* 125, 70–77. doi:10.1115/1.  
362 1531112
- 363 Yamaguchi, G. T. and Zajac, F. E. (1989). enA planar model of the knee joint to characterize the knee  
364 extensor mechanism. *Journal of Biomechanics* 22, 1–10. doi:10.1016/0021-9290(89)90179-6
- 365 Young, F., Rode, C., Hunt, A., and Quinn, R. (2019). enAnalyzing Moment Arm Profiles in a Full-Muscle  
366 Rat Hindlimb Model. *Biomimetics* 4, 10. doi:10.3390/biomimetics4010010

## FIGURES

## TABLES

**Table 1.** Muscle origin and insertion locations for different models. Origin is in femur reference frame, insertion is in the tibia reference frame.

Muscle	Origin/Insertion	Model	X (m)	Y (m)	Z (m)
Flexor	origin	Pinned knee	-0.075	0.100	0.0328
Flexor	insertion	Pinned knee	-0.05011	-0.045	0.0326
Extensor	origin	Pinned knee	0.030	-0.050	0
Extensor	insertion	Pinned knee	0.0425	-0.076	0
Bifemsh	origin	Gait2392	0.005	-0.211	0.023
Bifemsh	insertion	Gait2392	-0.03	-0.036	0.029
Vastus int.	origin	Gait2392	0.029	-0.192	0.031
Vastus int.	insertion	Gait2392	moving	moving	0.0018
Flexor, 10 mm	origin	Biomimetic knee	-0.050	-0.045	0.0328
Flexor, 10 mm	insertion	Biomimetic knee	-0.0279	-0.046	0.0328
Extensor, 10 mm	origin	Biomimetic knee	0.040	0.035	0
Extensor, 10 mm	insertion	Biomimetic knee	0.021	-0.072	0
Flexor, 40 mm	origin	Biomimetic knee	-0.050	-0.045	0.0328
Flexor, 40 mm	insertion	Biomimetic knee	-0.0279	-0.046	0.0328
Extensor, 40 mm	origin	Biomimetic knee	0.040	0.035	0
Extensor, 40 mm	insertion	Biomimetic knee	0.022	-0.072	0